Journal of Solid State Chemistry **153,** 124–131 (2000)
doi:10.1006/jssc.2000.8761, available online at http://www.idealibrary.com on IDEAL®

Single Crystal Growth of the High Pressure Phase of $(VO)_2P_2O_7$ at 3 GPa

T. Saito,* T. Terashima,* M. Azuma*,† and M. Takano*,†

*Institute for Chemical Research, Kyoto University, Uji, Kyoto-fu 611-0011, Japan; and †CREST, Japan Science and Technology Corporation (JST), Kawaguchi, Saitama 332-0012, Japan

E-mail: saito@msk.kuicr.kyoto-u.ac.jp; terachan@msk.kuicr.kyoto-u.ac.jp; masaki@scl.kuicr.kyoto-u.ac.jp; takano@scl.kyoto-u.ac.jp

T. Goto‡ and H. Ohta‡,§

‡Department of Physics, Faculty of Science, Kobe University, 1-1 Rokkodai, Nada, Kobe 657-8501, Japan, and §Venture Business Laboratory, Kobe University, 1-1 Rokkodai, Nada, Kobe 657-8501, Japan

E-mail: gotoh@phys.sci.kobe-u.ac.jp; ohta@phys.sci.kobe-u.ac.jp

W. Utsumi

Department of Synchrotron Radiation Research, Japan Atomic Energy Research Institute, 1-1-1 Kouto, Mikazuki, Sayo, Hyougo 679-5148, Japan

E-mail: utsumi@sp8sun.spring8.or.jp

P. Bordet

Laboratoire de Cristallographie, CNRS, BP 166, 38042 Grenoble Cedex 9, France

E-mail: bordet@labs.polycnrs-gre.fr

and

D. C. Johnston

Ames Laboratory and Department of Physics and Astronomy, Iowa State University, Ames, Iowa 50011

E-mail: johnston@ameslab.gov

Received February 29, 2000; in revised form April 28, 2000; accepted May 4, 2000; published online July 11, 2000

Single crystals of the high-pressure phase of $(VO)_2P_2O_7$ were grown by slowly cooling the melt at 3 GPa. Relevant reactions at high pressure and high temperature were studied in advance by *in situ* X-ray diffraction (XRD) measurements. The crystal structure of the high-pressure phase was determined by single-crystal XRD. Magnetic susceptibility of the crystal was measured along the three principal axes and analyzed using a $S=\frac{1}{2}$ Heisenberg AF alternating-exchange chain model. A good fit was obtained using the g values determined by ESR measurements, $J_1/k_B = 131.6(1)$ K, and an alternation parameter of $\alpha \equiv J_2/J_1 = 0.8709(5)$. The spin gap was estimated to be $\Delta/k_B = 33.4(2)$ K.

Key Words: **high-pressure synthesis; single crystal; synchrotron XRD; ESR; magnetic susceptibility; $S=\frac{1}{2}$ Heisenberg AF alternating-exchange chain.**

1. INTRODUCTION

High-pressure (HP) synthesis is a powerful method to search for new materials. It should be noted that several new low-dimensional quantum spin compounds such as high-T_C superconductors and spin ladders have been synthesized at HP in the past decade (1–5). One of these is the HP-phase of $(VO)_2P_2O_7$ (HP-VOPO) which is a one-dimensional (1D) antiferromagnet stabilized at 3 GPa (6). VOPO prepared at ambient pressure (AP) shows several modifications (7), some of which have long been known as effective catalysts for oxidation of *n*-butane to maleic anhydride (8, 9). Among them, α-$(VO)_2P_2O_7$ (AP-VOPO) has attracted attention also for its interesting magnetic properties.

AP-VOPO is made of VO_5 pyramids and PO_4 tetrahedra, and the vanadium ions are in an oxidation state of $4+$ with spin $\frac{1}{2}$ (10, 11). Johnston *et al.* found that the

0022-4596/00 $35.00

magnetic ground state is a singlet one and explained the temperature dependence of the magnetic susceptibility using a $S = \frac{1}{2}$ Heisenberg AF alternating-exchange chain model (12). Subsequently, however, a two-leg ladder model (13, 14) was found to be applicable as well, the ladder having almost straight V–O–V bonds in the leg direction and two orthogonal V–O–V bonds in the rung direction. However, a recent neutron-scattering study on single crystals revealed that AP-VOPO is best described as an AF alternating spin chain system with the chains running along the "rung" direction (15). The interaction along the "leg" was found to be ferromagnetic. According to the neutron-scattering study, the major AF interaction (J_1) between a pair of VO_5 pyramids is mediated by the PO_4 tetrahedra, while the seemingly strong interaction between a pair of edge-sharing VO_5 pyramids (J_2) is of minor importance in fact. The neutron data also revealed that there were two spin gaps of 36 and 67 K, which matched a theoretical prediction that the second gap due to the two-magnon excitation should be twice as large as the first one (16). However, there are two kinds of slightly different chains in AP-VOPO (11), which makes it difficult to identify the origin of the second gap, that is, it is difficult to judge whether both chains have the same double gaps or each one has a different single gap. Recent NMR and magnetization studies indicated that the latter is the case (17, 18).

In a previous paper we reported that AP-VOPO transforms into a simplified structure containing only one kind of such chains (see Fig. 1) on annealing under high pressure (2–3 GPa) (6). The magnetic susceptibility and heat capacity measurements indicated only one spin gap, the second one being unobservable in the magnetization curve up to 60 T (6). This is consistent with the above-mentioned studies on AP-VOPO (17, 18) indicating the absence of the second gap owing to the two-magnon excitation.

In this paper, we report a direct observation of the AP–HP transformation and also the melting by means of powder XRD study at high pressure and high temperature. On the basis of these results, single crystals of the HP phase were grown at 3 GPa. Single-crystal XRD was done for structural analysis. ESR and magnetic susceptibility were measured along the a, b, and c axes of the orthorhombic structure, and the data were fitted (19) by the $S = \frac{1}{2}$ Heisenberg AF alternating-exchange chain model using quantum Monte Carlo simulations and transfer-matrix density-matrix renormalization group calculations (20).

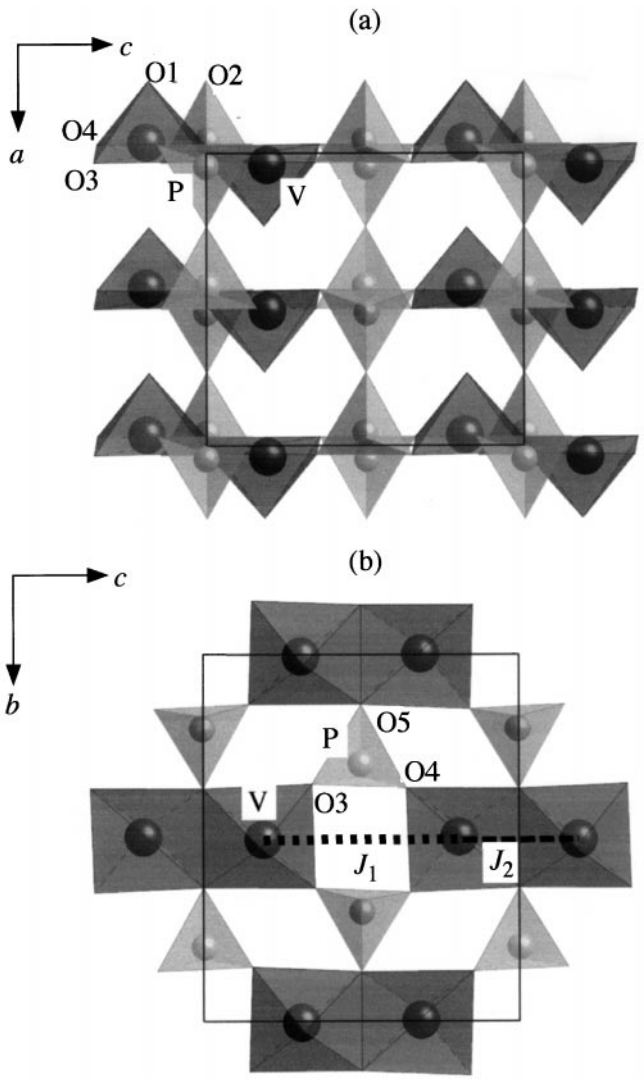

FIG. 1. Crystal structure of HP-VOPO viewed along the b axis (a) and the a axis (b). The large and small circles represent vanadium and phosphorous atoms, respectively. Oxygen atoms are placed at the vertexes of the polyhedra. J_1 and J_2 ($J_1 > J_2 = \alpha J_1$) represent the superexchange interactions between V^{4+} ions.

2. EXPERIMENTAL PROCEDURES

The starting material, AP-VOPO, was prepared from NH_4VO_3 and $NH_4H_2PO_4$. Stoichiometric amounts of these compounds were mixed, pressed into pellets and then heated at 550, 600, 700, and 750°C successively for 12 h each, and finally at 850°C for 24 h with intermediate grinding and pelletization. All of these heat treatments were done in flowing CO_2. The crystal structure and the magnetic property of the polycrystalline AP-VOPO sample thus obtained were reported elsewhere (11).

An XRD study under high pressure was carried out at SPring-8, Japan Synchrotron Radiation Research Institute. Because the oxidation state of vanadium is very sensitive to the atmosphere during heat treatment, a powder sample of AP-VOPO was filled in a platinum capsule (ϕ 4 mm × 6 mm) and then compressed in a conventional cubic anvil-type apparatus (SMAP 180) placed at beam line BL14B1. The sample was irradiated with white X-rays, and the transmitted beam was detected by a solid state detector fixed at

$2\theta = 3.973°$. The sample was first compressed to 3 GPa at room temperature and then heated stepwise.

Single crystals of HP-VOPO were grown in another apparatus by slowly cooling the melt at 3 GPa as will be described here. AP-phase powder filled in a platinum capsule (ϕ 6 mm × 9 mm) was compressed to 3 GPa and then heated up to 1180°C in 15 min. After being held at this temperature for 10 min, the sample was first cooled down to 680°C in 60 h and then down to room temperature in 5 h.

The crystal structure was refined using 4-axis XRD on a piece of spherically shaped single crystal of about 0.15 mm in radius. Two sets of data were collected at different detector angle on a κ-ccd diffractometer up to $2\theta = 89°$. About 23,000 reflections, including 3557 independent reflections, were observed with $F > 3\sigma(F)$ after average (R merge = 5%). The refinement started from the previously obtained powder data (6), and it converged to an R factor of 4.22%.

X-band ESR measurements were performed with a Bruker EPR spectrometer EMX081 using a TE103 rectangular cavity. The frequency of the microwave was approximately 9.4 GHz. The magnetic field was swept from 3150 to 3850 G, and the resolution of the data point was 0.2 G. An NMR gaussmeter was used to calibrate the magnetic field. The amplitude of the modulation field was 5 G, which was smaller than the sample's linewidth of 30 G. The angular dependence measurement was performed by using a programmable goniometer with an angular resolution of 0.125°, and the data were taken every 5°. The temperature-dependence measurements were performed from 3.5 to 300 K using an Oxford Instruments He flow cryostat. The magnetic susceptibility was measured for a pair of samples in an external magnetic field of 1 T from 2 to 300 K with a SQUID magnetometer (Quantum Design MPMS XL). One of the samples was a piece of single crystal (0.26 mg), and the other was powdered single crystals.

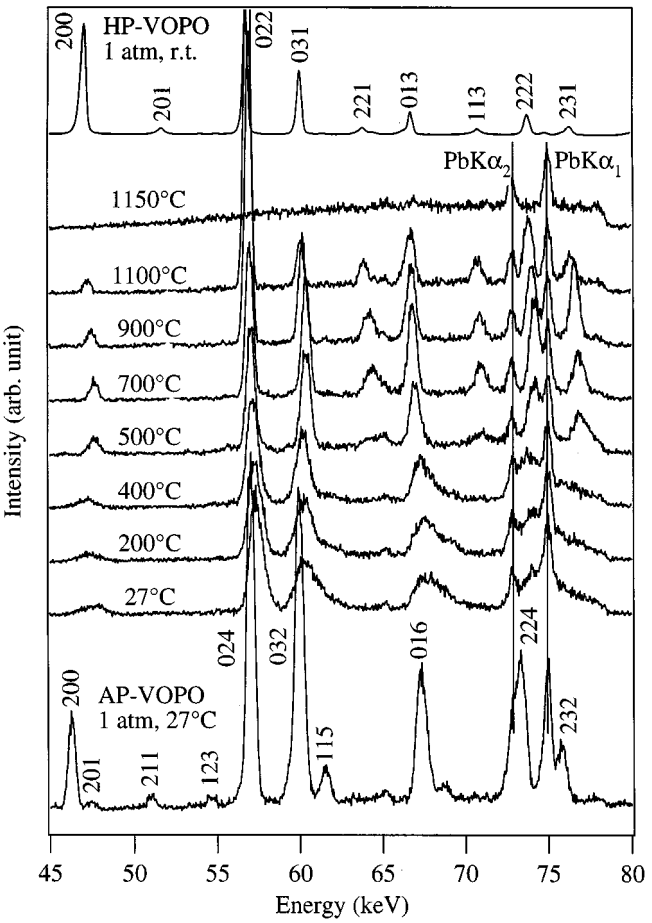

FIG. 2. Synchrotron XRD patterns of HP-VOPO at various temperatures at 3 GPa. The pattern at the top was taken using Cu$K\alpha_1$ radiation at room temperature and 1 atm, and the pattern at the bottom is that of AP-VOPO taken using synchrotron radiation at room temperature and 1 atm. The two vertical lines in the figure stand for the characteristic X rays of Pb ($K\alpha_1$, $K\alpha_2$) generated from the beam stopper, and the drop near 78 keV corresponds to the absorption edge of Pt used as the capsule.

3. RESULTS AND DISCUSSIONS

3.1. XRD Measurement at High Pressure

Powder XRD patterns of HP-VOPO collected at various temperatures between 27 and 1170°C at 3 GPa are shown in Fig. 2. The two vertical lines at 72.9 and 75.1 keV stand for the characteristic X rays of Pb ($K\alpha_1$, $K\alpha_2$) generated from the beam stopper. The drop near 78 keV corresponds to the absorption edge of Pt used as the sample capsule. The pattern at the bottom is that of the starting material, AP-VOPO, taken at room temperature and 1 atm. Compared with this, peak shifts to the high-energy side are clearly seen in the data taken at 3 GPa, which indicate a lattice shrinkage under pressure. Another characteristic feature of the pattern at 3 GPa is peak broadening, likely due to lattice strain and also to the small particle size of the crushed powder. In any case, the pattern at 3 GPa could still be indexed assuming the AP structure.

When the temperature was increased, all the peaks shifted a little to the low-energy side because of thermal expansion and, at the same time, sharpened gradually because of recrystallization. The transition to the HP phase was observed between 400 and 500°C, and all the peaks could be assigned to the HP phase above 500°C. The pattern of a powder HP-phase sample, which was taken at 27°C and 1 atm with Cu$K\alpha_1$ radiation and converted using a relation $E = 12.39/\lambda$ (keV), is shown at the top of Fig. 2 for comparison.

The lattice constants at 3 GPa calculated from the peak positions are plotted in Fig. 3 against temperature. The c axis length below 500°C was halved in the figure for the sake of comparison because the unit cell of the less symmetric AP phase is essentially twice as large as that of the HP phase in that direction. There is a discontinuity between 400

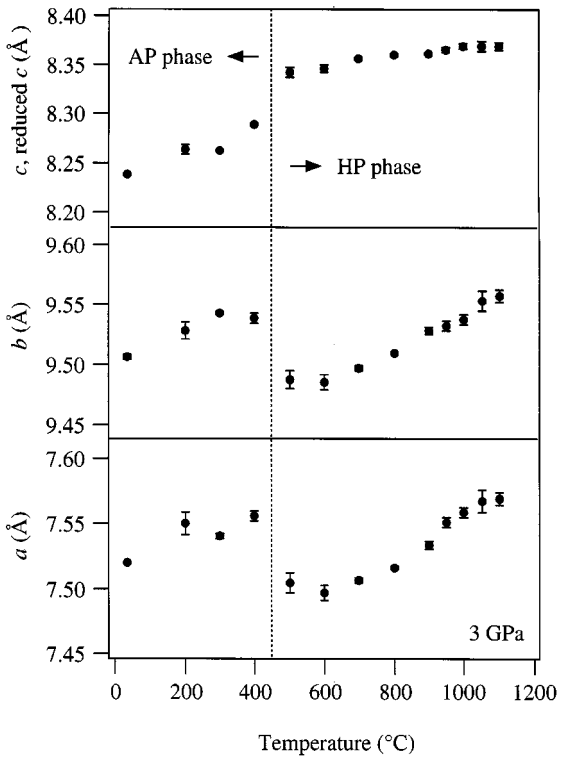

FIG. 3. Lattice parameters of AP- and HP-VOPO at various temperatures and 3 GPa. The dotted line represents the boundary between the AP and HP phases. The c axis length is halved below 500°C for the sake of comparison, because the unit cell of the less symmetric AP phase is essentially twice as large as that of the more symmetric HP phase in that direction.

and 500°C in every direction, indicating the occurrence of the phase transition in this temperature range. The HP phase changed its lattice parameters continuously up to 1100°C and then disappeared. The melting point of HP-VOPO at 3 GPa was thus determined to be between 1100 and 1150°C.

3.2. *Single-Crystal Growth and Structure Refinement*

It is known that AP-VOPO melts congruently and that green crystals grow by slow cooling under controlled oxygen fugacity (21). The crystal growth at 3 GPa could be done similarly if the slow cooling process was continued down to 800°C or less. The products quenched from above 800°C were all blackish and glassy. This is similar to AP-VOPO, which tends to vitrify because of its high viscosity (21). Green transparent platelike single crystals of HP-VOPO were obtained by cooling from 1180 to 680°C in 60 h and then to room temperature in 5 h. The typical size of the crystals was 1 mm × 0.5 mm × 0.2 mm (see Fig. 4). The wide crystal surface was found to be parallel to the 011 plane by two axes XRD which showed only $0nn$ ($n = 1, 2, 3, 4$) reflection peaks. The 011 plane is at an angle of about 49° with the V^{4+} spin chain.

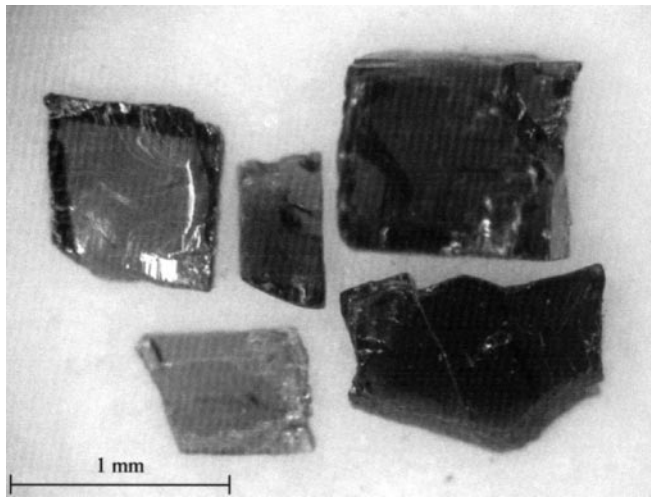

FIG. 4. Magnified view of the grown single crystals of HP-VOPO.

The crystallographic data, data collection parameters, and final refinement conditions are summarized in Table 1, and the final atomic coordinates are given in Table 2. The anisotropic thermal parameters are listed in Table 3 and shown schematically in Fig. 5. The selected bond lengths, atomic distances, and bond angles are given in Tables 4

TABLE 1
Crystal Data, Data Collection Parameters, and Final Refinement Conditions

Crystal data	
Chemical formula	$V_2P_2O_9$
Formula weight (g/mol)	307.825
Space group	*Pnab* (No. 60)
a (Å)	7.571(1)
b (Å)	9.536(1)
c (Å)	8.362(1)
Cell volume (Å^3)	603.7
Z	4
Calculated density (g/cm^3)	3.386
Data collection	
Crystal size (mm)	spherical, radius ~0.15
Radiation	Ag$K\alpha$
Wavelength (Å)	0.56080
Extinction model	Isotropic, type 1, Gaussian
Number of reflection measured	~23,000
Number of unique reflections	3557
Criterion for observed reflections	$F > 3\sigma(F)$
2θ maximum (degree)	89
Structure refinement	
Refinement on	F
R, R_w (%)	4.22, 4.02
Weighting scheme	$w = 1/\sigma^2$
Number of refined parameters	61
Goodness-of-fit	2.76

TABLE 2
Atomic Coordinates

Atom	Wyckoff position	Fractional atomic coordinates		
		x	*y*	*z*
V	8*d*	0.038310(9)	0.003746(6)	0.310363(8)
P	8*d*	0.045157(13)	0.201895(11)	0.002421(11)
O1	8*d*	0.247719(49)	0.02840(40)	− 0.318373(40)
O2	4*c*	0.250000(0)	0.169244(55)	0.000000(0)
O3	8*d*	− 0.032295(44)	0.136508(34)	− 0.145055(36)
O4	8*d*	0.530822(47)	0.147620(33)	− 0.155618(37)
O5	8*d*	− 0.025504(42)	0.135671(33)	− 0.499776(26)

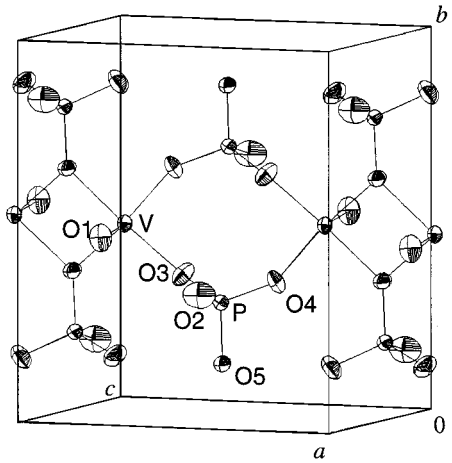

FIG. 5. ORTEP drawing of the HP-VOPO structure.

and 5, respectively. The result of this structure refinement is in good agreement with that obtained by a Rietveld analysis of powder XRD and neutron diffraction data reported previously (6). Comparing the lattice constants of the AP and HP phases, we notice that the *a* and *b* axes of the HP phase are slightly shorter than those of the AP phase and that the *c* axis is slightly longer than one half of that of the AP phase. As a whole, the density of the HP phase is 1.9% larger than that of the AP phase at room temperature and ambient pressure.

3.3. Magnetic Measurements

The principle *g* values of HP-VOPO were determined by the ESR angular dependence measurements of the single crystal at room temperature and the results are shown in Fig. 6. Obtained *g* values are $g_a = 1.928(1)$, $g_b = 1.974(1)$, and $g_c = 1.971(1)$. We also performed the temperature dependence measurements from 3.5 to 300 K for $H_{\|a}$, $H_{\|b}$, and $H_{\|c}$. The temperature dependence of the integrated intensity for $H_{\|b}$ is shown in Fig. 7, and those for $H_{\|a}$ and $H_{\|c}$ exhibited similar behavior.

The magnetic susceptibility χ of HP-VOPO measured along the *a*, *b*, and *c* axes are plotted vs temperature *T* in Fig. 8. The data can be expressed as

$$\chi(T) = \chi_0 + \frac{C_{\text{imp}}}{T - \theta_{\text{imp}}} + \chi^{\text{spin}}(T), \qquad [1]$$

where the first term, χ_0, is the sum of the nearly isotropic orbital diamagnetic atomic core contribution, χ^{core}, and the normally anisotropic orbital paramagnetic Van Vleck contribution, χ^{VV}, which are both normally nearly independent of *T*. The second term is an extrinsic impurity Curie–Weiss term, χ_{imp}, with an impurity Curie constant C_{imp} and a Weiss temperature θ_{imp} which gives rise to a low-temperature upturn in $\chi(T)$ that is not predicted by theory for the third term, the intrinsic spin susceptibility, $\chi^{\text{spin}}(T)$, and is assumed to arise from finite chain segments containing an odd number of spins, impurity-phase intergrowth in the crystals, paramagnetic impurities, and/or defects.

Due to the small mass of the crystal and the uncertainty in the sample holder correction relative to the sample signal, the measured data were normalized to the data obtained

TABLE 3
Anisotropic Thermal Parameters

Atom	U_{11}	U_{22}	U_{33}	U_{12}	U_{13}	U_{23}	U_{iso}
V	0.4742(32)	0.4910(27)	0.3647(36)	0.0026(17)	− 0.0078(17)	− 0.0009(15)	0.4433(19)
P	0.5553(46)	0.3973(40)	0.4041(48)	− 0.0023(25)	0.0143(31)	0.0068(24)	0.4522(26)
O1	0.6256(109)	1.2701(129)	0.9236(136)	− 0.0884(107)	0.0000(108)	0.0421(98)	0.9398(72)
O2	0.5255(156)	1.1689(184)	2.0113(232)	0.0000(0)	− 0.0844(163)	0.0000(0)	1.2352(112)
O3	1.0127(138)	0.9051(111)	0.7586(122)	0.0696(94)	− 0.1105(101)	− 0.3599(88)	0.8921(72)
O4	1.4374(154)	0.8421(110)	0.6587(114)	0.0285(100)	0.2558(111)	− 0.2852(88)	0.9794(74)
O5	1.0963(113)	0.4344(99)	0.4766(119)	0.0624(79)	− 0.0561(112)	− 0.0051(66)	0.6691(64)

Note. Values above are given in units of 10^{-2} Å^2.

TABLE 4
Selected Bond Lengths

Atoms	Distance (Å)	Atoms	Distance (Å)
V–O1	1.6042(4)	P–O2	1.5819(1)
V–O1	2.2223(4)	P–O3	1.5011(3)
V–O3	1.9492(3)	P–O4	1.4966(3)
V–O4	1.9393(3)	P–O5	1.5562(3)
V–O5	2.0796(3)		
V–O5	2.0730(3)		

for large polycrystalline sample of crushed single crystals (χ_{powder}) as follows. All the data for a, b, and c axes were averaged at each temperature (χ_{ave}) and then compared with χ_{powder}, which matched very well with $0.99\chi_{ave} - 2.04 \times 10^{-4}$ emu/mol V above 50 K. Below that temperature, χ_{powder} was larger than the corrected single-crystal data, which may be due to the extrinsic impurity Curie–Weiss term χ_{imp}. The magnetic susceptibility data for the a, b, and c axes were corrected by the same equation above. The multiplicative factor in the equation compensates the mass error, and the additive one may be the sample holder contribution. The temperature dependence of the magnetic susceptibility data thus obtained, χ_a, χ_b, and χ_c, is very similar, but χ_b and χ_c are 2–4% larger than χ_a, which is consistent with the ESR measurement above.

In the previous analysis of the susceptibility, the data from the powder sample were of poor quality, the amount of χ_{imp} being about 3 times of the present data. Also, the fit was performed in a limited temperature range above 30 K. The fit yielded $J_1 = 136$ K, and $\alpha = 0.9$, which gave the spin gap value of 28.4 K, but the reliability was not sufficient for the

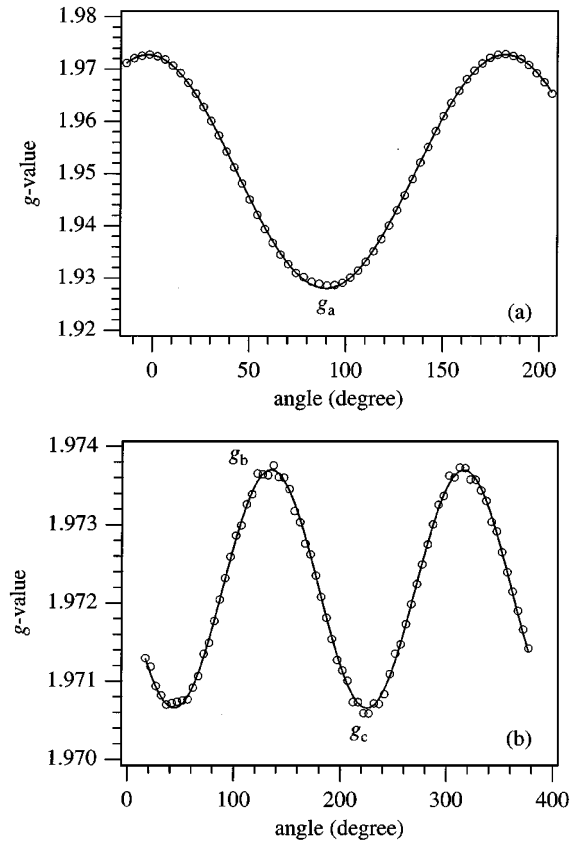

FIG. 6. Angle dependence of the g value for a single crystal of HP-VOPO. The single crystal was rotated around the $01\bar{1}$ direction (a), which is perpendicular to the wide crystal surface, and the a axis (b).

TABLE 5
Selected Atomic Distances and Bond Angles

Atoms		Direction	Distance (Å)
V–O4–P–O5–V		Interchain	4.8737(1), 6.4216(1)
V–O3–P–O5–V		Interchain	4.8737(1), 6.3147(1)
V–O3–P–O4–V		J_1	5.2233(1)
V–O5–V		J_2	3.2249(1)
Bond	Angle (degree)	Bond	Angle (degree)
V–O3–P	138.18(2)	O3–V–O5	94.79(1)
V–O4–P	147.11(2)	O3–V–O5	161.23(1)
V–O5–P	127.98(1)	O4–V–O5	162.11(1)
V–O5–P	130.01(1)	O4–V–O5	91.85(1)
O1–V–O1	175.85(2)	O4–V–O5	162.11(1)
O1–V–O3	101.86(2)	O4–V–O5	91.85(1)
O1–V–O3	80.76(1)	O5–V–O5	78.10(1)
O1–V–O4	99.55(2)	O2–P–O3	106.90(2)
O1–V–O4	83.60(1)	O2–P–O4	108.64(2)
O1–V–O5	96.27(2)	O2–P–O5	106.83(2)
O1–V–O5	96.21(2)	O3–P–O4	114.17(2)
O1–V–O5	80.24(1)	O3–P–O5	111.49(2)
O1–V–O5	80.92(1)	O4–P–O5	108.52(2)
O3–V–O4	90.13(4)		

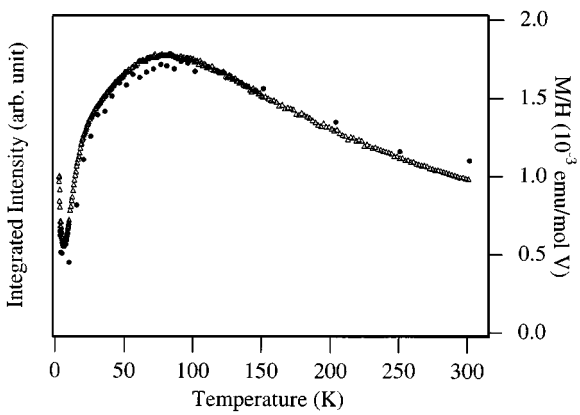

FIG. 7. Temperature dependence of the integrated ESR intensity for $H_{\|b}$ (●). Susceptibility data are also plotted for comparison (△).

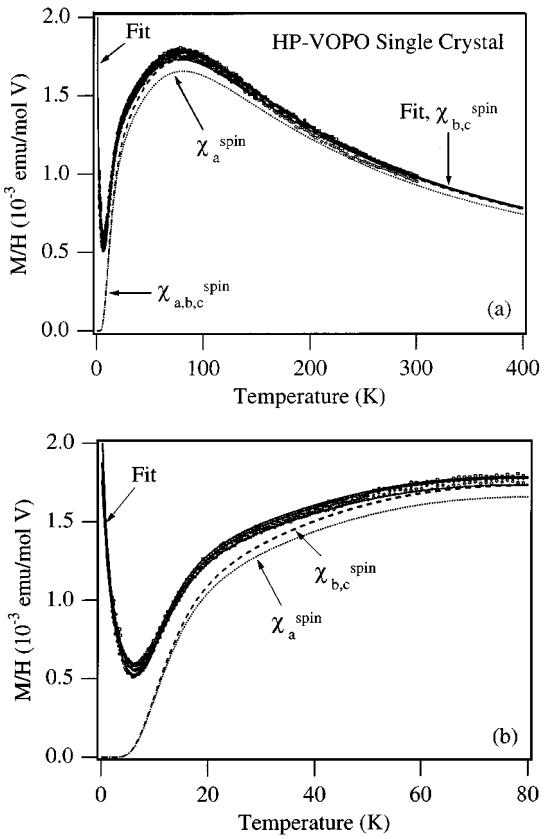

FIG. 8. (a) Magnetic susceptibility χ versus temperature T for a single crystal of HP-VOPO along the a axis (○), b axis (●), and c axis (□) from 2 to 300 K. (b) Expanded plot of the data below 80 K. In both (a) and (b), the set of three solid curves is a four-dimensional fit to all data points for the three directions (see text). The dashed curves represent the intrinsic spin susceptibility for the $\alpha = a$ axis (short dash) and b and c axes (longer dash); the fitted $\chi_b^{spin}(T)$ and $\chi_c^{spin}(T)$ are indistinguishable from each other in this scale.

reasons above. The susceptibility data with a small χ_{imp} were then analyzed in the whole temperature range (19), and the results are plotted in Fig. 8 with solid lines. $\chi_{spin}(T)$ data were also calculated and are plotted with dashed lines. The temperature dependence of these data was fit by the $S = \frac{1}{2}$ Heisenberg AF alternating-exchange chain model, using quantum Monte Carlo simulations and transfer-matrix density-matrix renormalization group calculations (20), which gave a very good fit. The obtained $J_1 = 131.6(1)$ K and $\alpha = 0.8709(5)$ gave a spin gap value of 33.4(2) K.

Although the temperature dependence of the magnetic susceptibility of HP-VOPO showed a good agreement with the $S = \frac{1}{2}$ Heisenberg AF alternating-exchange chain model, the magnitude of the spin gap of this compound estimated by magnetization measurement was considerably smaller than the one calculated here, only 23 K (6). Besides, the crystal structure of HP-VOPO suggests the possibility of other exchange interactions present in the system. For example, the bond length and the angles of the V–O(3)–P–O(5)–V path connecting two chains in the c direction are similar to those mediating J_1 exchange (V–O(3)–P–O(4)–V) as listed in the table. These suggest that the AF interactions along the c axis may not be negligible. To answer this question, exchange interactions should be determined by means of inelastic neutron-scattering study on the obtained single crystals.

4. CONCLUSION

VOPO was found to transform from the AP phase into the HP phase between 400 and 500°C at 3 GPa and melt between 1100 and 1150°C under the pressure. Single crystals of the HP phase were grown by slow cooling of the melt at 3 GPa, and the crystal structure was determined by single-crystal XRD. The wide surface of the crystals was parallel to the 011 plane, which makes an angle of about 49° with the spin chains. Principle g values of a single crystal were determined by ESR measurements, which gave $g_a = 1.928(1)$, $g_b = 1.974(1)$, and $g_c = 1.971(1)$. The magnetic susceptibility of a single crystal was measured with the external field parallel to the a, b, and c axes and was fitted to the $S = \frac{1}{2}$ Heisenberg AF alternating-exchange chain model. The fit yielded $\alpha \equiv J_2/J_1 = 0.8709(5)$ and $J_1/k_B = 131.6(1)$ K. The size of the spin gap estimated from these parameters was 33.4(2) K, which is considerably larger than the one estimated from the magnetization measurement on powder samples. This difference might be due to the neglect of the interchain magnetic interactions. The technique established in this study, the combination of HP XRD with HP single-crystal growth, should be applied to other HP-phases exhibiting exotic properties.

ACKNOWLEDGMENTS

This work was partly supported by a grant for Core Research for Evolutional Science and Technology (CREST) of Japan Science and Technology Corporation (JST) and also Grant-in Aid for Scientific Research of Ministry of Education, Science, Sports and Culture, Japan. The alignment of the crystals used for magnetic measurements was performed by J. Yamaura at ISSP, University of Tokyo. The synchrotron radiation experiments were performed at the SPring-8 with the approval of the Japan Synchrotron Radiation Research Institute (Proposal No. 1999B0381-ND-np). Ames Laboratory is operated for the U.S. Department of Energy by Iowa State University under Contract No. W-7405-Eng-82. The work at Ames was supported by the Director for Energy Research, Office of Basic Energy Sciences.

REFERENCES

1. M. Takano, Z. Hiroi, S. Kawasaki, R. Kannno, and T. Takeda, Springer Series in Solid-State Sciences, Vol. 125, Physics and Chemistry of Transition-Metal Oxides, Springer-Verlag, Berlin, 1999.
2. Z. Hiroi, N. Kobayashi, and M. Takano, *Nature* **371,** 139 (1994).

3. Z. Hiroi and M. Takano, *Nature* **377,** 41 (1995).
4. M. Azuma, Z. Hiroi, M. Takano, K. Ishida, and Y. Kitaoka, *Phys. Rev. Lett*. **73,** 3463 (1994).
5. M. Azuma, S. Kaimori, and M. Takano, *Chem. Mater*. **10,** 3124 (1998).
6. M. Azuma, T. Saito, Y. Fujishiro, Z. Hiroi, M. Takano, F. Izumi, T. Kamiyama, T. Ikeda, Y. Narumi, and K. Kindo, *Phys. Rev. B* **60,** 10145 (1999).
7. E. Bordes and P. Courtine, *J. Chem. Soc., Chem. Commun.* **294** (1985).
8. E. Bordes, P. Courtine, and J. W. Johnson, *J. Solid State Chem.* **55,** 270 (1984).
9. P. L. Gai and K. Kourtakis, *Science* **267,** 661 (1995).
10. P. T. Nguyen, A. W. Sleight, N. Roberts, and W. W. Warren, *J. Solid State Chem.* **122,** 256 (1996).
11. Z. Hiroi, M. Azuma, Y. Fujishiro, T. Saito, M. Takano, F. Izumi, T. Kamiyama, and T. Ikeda, *J. Solid State Chem.* **146,** 369 (1999).
12. D. C. Johnston, J. W. Johnston, D. P. Goshorn, and A. J. Jacobson, *Phys. Rev. B* **35,** 219 (1987).
13. E. Dagotto, J. Riera, and D. Scalapino, *Phys. Rev. B* **45,** 5744 (1992).
14. T. Barnes and J. Riera, *Phys. Rev. B* **50,** 6817 (1994).
15. A. W. Garrett, S. E. Nagler, D. A. Tennant, B. C. Sales, and T. Barnes, *Phys. Rev. Lett*. **79,** 745 (1997).
16. G. S. Uhrig and H. J. Schulz, *Phys. Rev. B* **54,** R9624 (1996).
17. T. Yamauchi, Y. Ueda, Y. Narumi, K. Tatani, K. Kobayashi, K. Kindo, J. Kikuchi, and K. Motoya, *Phys. Rev. Lett*. **83,** 3729 (1999).
18. J. Kikuchi, K. Motoya, T. Yamauchi, and Y. Ueda, *Phys. Rev. B* **60,** 6731 (1999).
19. D. C. Johnston, T. Saito, M. Azuma, M. Takano, T. Yamauchi, and Y. Ueda, *Phys. Rev. B*, submitted.
20. D. C. Johnston, R. K. Kremer, M. Troyer, X. Wang, A. Klümper, S. L. Bud'ko, A. F. Panchula, and P. C. Canfield, *Phys. Rev. B* **61,** 9558 (2000).
21. A. V. Prokofiev, F. Büllesfeld, W. Assmus, H. Schwenk, D. Wichert, U. Löw, and B. Lüthi, *Eur. Phys. J. B* **5,** 313 (1998).